

Jet energy scale setting with " $\gamma + Jet$ " events at LHC energies.

Event rates, P_t structure of jet.

D.V. Bandourin^{1†}, V.F. Konoplyanikov^{2*}, N.B. Skachkov^{3†}

E-mail: (1) dmv@cv.jinr.ru, (2) kon@cv.jinr.ru, (3) skachkov@cv.jinr.ru

† Laboratory of Nuclear Problems

** Laboratory of Particle Physics*

Abstract

In this paper the study of " $\gamma + Jet$ " events is continued, aimed at jet energy scale setting and hadron calorimeter calibration at LHC energies. The event number distribution over P_t^γ and η^γ is presented. The features of " $\gamma + Jet$ " events in the barrel region of CMS detector ($|\eta| < 1.4$) are exposed. P_t structure of the region in the $\eta - \phi$ space inside and beyond jet is also shown.

1. INTRODUCTION

In this paper we continue the study of " $\gamma + Jet$ " process, started in [1] aimed at jet energy scale setting and hadron calorimeter calibration at LHC energies.

This article is organized in the following way. In Section 2 we shall estimate the event number distribution dependence on a value of "back-to-back" $\phi_{(\gamma, jet)}$ angle between the direct photon \vec{P}_t^γ and jet \vec{P}_t^{Jet} and on the P_t of the initial state radiation (ISR), i.e. P_t^{ISR} value. P_t^γ and η^γ dependence of rates is also studied in this section. Estimation of " $\gamma + Jet$ " event rates for Barrel (HB), Endcap (HE) and Forward (HF) parts of hadron calorimeter (HCAL) is performed in the last subsection of Section 2. In Section 3 we consider the " $\gamma + Jet$ " event features in HB region. In particular, we study the P_{tCUT}^{clust} parameter influence on the selection of events with a good photon and jet P_t balance and also the problem of selection of events with suppressed ISR activity. The next subsections are devoted to the P_t structure of jets in $\eta - \phi$ space and to the particles P_t distribution inside and beyond the jet.

2. EVENT RATES FOR DIFFERENT P_t^γ AND η^γ INTERVALS.

2.1 Event number distribution dependence on "back-to-back" $\phi_{(\gamma, jet)}$ angle and on P_t^{ISR} values.

The definitions of observable physical variables introduced in Section 3.2 of [1] allow us to make the first step in the study of a possible way to select the events with a good P_t^γ and P_t^{Jet} balance. Here we shall study the spectrum of P_t56 variable (that is proportional to P_t^{ISR} up to the value of intrinsic parton transverse momentum inside a proton) in signal events with direct photons and this spectrum dependence on some of experimentally measurable variables. For this reason the results of 10^7 " $\gamma + Jet$ " events generation for every of four P_t^γ intervals (40–50, 100–120, 200–240, 300–360 GeV/c) by use of PYTHIA with account of 2 QCD subprocesses $q\bar{q} \rightarrow g + \gamma$ and $qg \rightarrow q + \gamma$ were analyzed. For this analysis the observables and the "Selection 1" cuts (1–7), defined in Sections 3.2 of [1], with the following cut parameters:

$$P_{tCUT}^{isol} = 5 \text{ GeV}/c; \quad \epsilon_{CUT}^\gamma = 7\%; \quad \Delta\phi < 15^\circ; \quad P_{tCUT}^{clust} = 20 \text{ GeV}/c. \quad (1)$$

were used. The value of the luminosity was taken to be $L = 10^{33} \text{ cm}^2 \text{ sec}^{-1}$ (low LHC luminosity).

In Tables 1, 2 and 4, 5 we present P_t56 spectra for two most illustrative cases of P_t^γ intervals: $40 < P_t^\gamma < 50 \text{ GeV}/c$ (Table 1 and 2) and $200 < P_t^\gamma < 240 \text{ GeV}/c$ (Table 4 and 5). The distributions of the number of events for integrated luminosity $L_{int} = 3 \text{ fb}^{-1}$ in different intervals of P_t56 ($\langle k_T \rangle$ was taken to be fixed at PYTHIA default value, i.e. $\langle k_T \rangle = 0.44 \text{ GeV}/c$) and for different "back-to-back" angle intervals $\phi_{(\gamma, jet)} = 180^\circ \pm \Delta\phi$ ($\Delta\phi = 15^\circ, 10^\circ$ and 5° as well as without any restriction on $\Delta\phi$, i.e. for the whole ϕ interval $\Delta\phi = 180^\circ$)¹ are given there. Tables 1 and 2 correspond to the case $P_{tCUT}^{clust} < 20 \text{ GeV}/c$ and serve as an illustration since it is rather a weak cut condition, while Tables 4 and 5 correspond to a more restrictive selection cut value $P_{tCUT}^{clust} = 5 \text{ GeV}/c$.

Firstly from the last summary lines of Tables 1–4 we can make a general conclusion about the $\Delta\phi$ -dependence of the events spectrum. Thus, in the case of weak restriction

¹The value $\Delta\phi = 5^\circ$ coincides with one CMS HCAL tower size in the ϕ -plane. and, thus, defines the precision of experimental registration of the jet \vec{P}_t vector.

$P_t^{clust} < 20 \text{ GeV}/c$ we can see from Table 1 that for the interval of $40 \leq P_t^\gamma \leq 50 \text{ GeV}/c$ there are about 66% of events concentrated in the $\Delta\phi < 15^\circ$ range, while 32% of events are in the $\Delta\phi < 5^\circ$ range. At the same time the analogous summary line of Table 2 shows us that at higher values $200 \leq P_t^\gamma \leq 240 \text{ GeV}/c$ the events spectrum moves to the small $\Delta\phi$ region: more than 99% of events have $\Delta\phi < 15^\circ$ and 79% of them have $\Delta\phi < 5^\circ$.

A tendency of very rapid concentration of the signal " $\gamma + Jet$ " event distributions with the growth of P_t^γ in a rather narrow back-to-back angle interval $\Delta\phi < 15^\circ$ becomes more distinctive with a more restrictive cut $P_{tCUT}^{clust} = 5 \text{ GeV}/c$ (see Tables 4 and 5). From the last summary line of the Tables 3 we see that in the case of $40 \leq P_t^\gamma \leq 50 \text{ GeV}/c$ more than 97% of the events have $\Delta\phi < 15^\circ$, while 68% of them are in the $\Delta\phi < 5^\circ$ range. At $200 \leq P_t^\gamma \leq 240 \text{ GeV}/c$ (see Table 5) more than 99% of the events that undergo this cut have $\Delta\phi < 5^\circ$. It means that imposing $P_{tCUT}^{clust} = 5 \text{ GeV}/c$ and suppressing cluster or mini-jet activity, we choose the events with a clean "back-to-back" (within 15°) topology of γ and jet orientation.

So, one can conclude that PYTHIA simulation predicts that at LHC energies most of the " $\gamma + Jet$ " events after imposing $P_{tCUT}^{clust} = 20 \text{ GeV}/c$ may have the vectors \vec{P}_t^γ and \vec{P}_t^{jet} being back-to-back within $\Delta\phi < 15^\circ$. The cut $P_{tCUT}^{clust} = 5 \text{ GeV}/c$ improves this tendency ².

It is worth mentioning that this picture reflects the predictions of one of the generators which are based on the approximate LO values for the cross section. It may change if the next-to-leading order or soft physics ³ effects are included and also after more real experimental data would be collected for comparison with a theory.

The other lines of the same Tables 1, 2 and 4, 5 contain the information about the P_{t56} (see formula (3) of [1]) spectrum that in reality corresponds approximately, up to the fixed value of $\langle k_T \rangle = 0.44 \text{ GeV}/c$, to the P_t^{ISR} spectrum.

From the comparison of Table 1 with Table 4 one can conclude that the most populated part of P_{t56} (or P_t^{ISR}) spectrum reduces practically by twice with restricting P_{tCUT}^{clust} . So for $\Delta\phi_{max} = 15^\circ$ we see that it drops from $0 < P_{t56} < 50 \text{ GeV}/c$ for $P_{tCUT}^{clust} = 20 \text{ GeV}/c$ to a more narrow interval of $0 < P_{t56} < 20 \text{ GeV}/c$ for the $P_{tCUT}^{clust} = 5 \text{ GeV}/c$ case. At higher P_t^γ interval for the same value $\Delta\phi_{max} = 15^\circ$ about the same factor 2 of P_{t56} spectrum reduction (from an interval $0 < P_{t56} < 50 \text{ GeV}/c$ for $P_{tCUT}^{clust} = 20 \text{ GeV}/c$ to a $0 < P_{t56} < 20 \text{ GeV}/c$ for $P_{tCUT}^{clust} = 5 \text{ GeV}/c$) can be found from the comparison of Table 2 with Table 5.

From the same tables one can also see that P_{t56} spectrum becomes slightly wider for higher values of P_t^γ : the dominant part of this spectrum in the interval $40 \leq P_t^\gamma \leq 50 \text{ GeV}/c$ spreads in the case of $P_{tCUT}^{clust} = 5 \text{ GeV}/c$ cut mainly within the interval $0 < P_{t56} < 10 \text{ GeV}/c$ with the maximum peak at $0 < P_{t56} < 5 \text{ GeV}/c$. At higher P_t^γ interval $200 \leq P_t^\gamma \leq 240 \text{ GeV}/c$, P_{t56} spectrum spreads out in a wider interval of $0 < P_{t56} < 15 \text{ GeV}/c$ having the peak of its maximum at $5 < P_{t56} < 10 \text{ GeV}/c$.

Thus, we can summarize that the PYTHIA generator used here predicts the values of P_t^{ISR} spectrum to increase while growing P_t^γ , but its contribution can be reduced by imposing a restrictive cut on the value of P_{tCUT}^{clust} (for more details see Section 3 and the following papers [2, 3]).

²The enlarging of P_t^γ values produces the same effect as it is seen from Tables 2 and 4 and will be demonstrated in more detail in our following papers [2, 3].

³We thank E. Pilon and J.Ph. Joliet for the information about new FNAL data on this subject and on the importance of NLO corrections and soft physics effects.

Table 1: Number of events dependence on P_{t56} and $\Delta\phi$ for $40 \leq P_{t\gamma} \leq 50 \text{ GeV}/c$ and $P_{t_{CUT}^{clust}} = 20 \text{ GeV}/c$ for $L_{int}=3fb^{-1}$

| P_{t56} (GeV/c) | $\Delta\phi_{max}$ | | | |
|---------------------------------|--------------------|------------|------------|-----------|
| | 180° | 15° | 10° | 5° |
| 0 – 5 | 1103772 | 1049690 | 1006627 | 849706 |
| 5 – 10 | 1646004 | 1564393 | 1403529 | 812304 |
| 10 – 15 | 1331589 | 1122473 | 771060 | 380122 |
| 15 – 20 | 992374 | 568279 | 365329 | 179767 |
| 20 – 25 | 725537 | 282135 | 183406 | 91113 |
| 25 – 30 | 559350 | 169186 | 112308 | 58395 |
| 30 – 40 | 911942 | 265961 | 178048 | 89867 |
| 40 – 50 | 388950 | 94112 | 62068 | 31000 |
| 50 – 100 | 91248 | 19442 | 12973 | 6234 |
| 100 – 300 | 34 | 0 | 0 | 0 |
| 300 – 500 | 0 | 0 | 0 | 0 |
| 0 – 500 | 7750799 | 5135671 | 4095348 | 2498507 |

Table 2: Number of events dependence on P_{t56} and $\Delta\phi$ for $200 \leq P_{t\gamma} \leq 240 \text{ GeV}/c$ and $P_{t_{CUT}^{clust}} = 20 \text{ GeV}/c$ for $L_{int}=3fb^{-1}$

| P_{t56} (GeV/c) | $\Delta\phi_{max}$ | | | |
|---------------------------------|--------------------|------------|------------|-----------|
| | 180° | 15° | 10° | 5° |
| 0 – 5 | 1429 | 1429 | 1427 | 1380 |
| 5 – 10 | 3266 | 3266 | 3264 | 3150 |
| 10 – 15 | 3205 | 3205 | 3200 | 3069 |
| 15 – 20 | 2827 | 2827 | 2819 | 2618 |
| 20 – 25 | 2409 | 2408 | 2393 | 1918 |
| 25 – 30 | 2006 | 2006 | 1982 | 1300 |
| 30 – 40 | 2608 | 2605 | 2533 | 1411 |
| 40 – 50 | 1237 | 1230 | 1067 | 586 |
| 50 – 100 | 1066 | 1018 | 842 | 536 |
| 100 – 300 | 313 | 307 | 293 | 221 |
| 300 – 500 | 0 | 0 | 0 | 0 |
| 0 – 500 | 20366 | 20301 | 19820 | 16189 |

Table 3: Number of events dependence on $\Delta\phi_{max}$ and on $P_{t\gamma}$ for $L_{int} = 3 \text{ fb}^{-1}$.
 $P_{t_{CUT}^{clust}} = 20 \text{ GeV}/c$ (summary)

| $P_{t\gamma}$ (GeV/c) | $\Delta\phi_{max}$ | | | |
|-------------------------------------|--------------------|------------|------------|-----------|
| | 180° | 15° | 10° | 5° |
| 40 – 50 | 7750799 | 5135671 | 4095348 | 2498507 |
| 100 – 120 | 323766 | 297323 | 258691 | 176308 |
| 200 – 240 | 20366 | 20301 | 19820 | 16189 |
| 300 – 360 | 3638 | 3638 | 3627 | 3323 |

Table 4: Number of events dependence on P_{t56} and $\Delta\phi$ for $40 \leq P_{t\gamma} \leq 50 \text{ GeV}/c$ and $P_{tCUT}^{clust} = 5 \text{ GeV}/c$ for $L_{int}=3fb^{-1}$

| P_{t56} (GeV/c) | $\Delta\phi_{max}$ | | | |
|----------------------|--------------------|--------|--------|--------|
| | 180° | 15° | 10° | 5° |
| 0 - 5 | 331522 | 331321 | 329876 | 295759 |
| 5 - 10 | 319153 | 318581 | 299960 | 187089 |
| 10 - 15 | 88603 | 82586 | 60537 | 32335 |
| 15 - 20 | 21244 | 15327 | 11663 | 6924 |
| 20 - 25 | 8101 | 5681 | 4639 | 2992 |
| 25 - 30 | 4739 | 3395 | 2823 | 1949 |
| 30 - 40 | 3495 | 2790 | 2555 | 1714 |
| 40 - 50 | 1647 | 1277 | 1042 | 471 |
| 50 - 100 | 101 | 67 | 67 | 67 |
| 100 - 500 | 0 | 0 | 0 | 0 |
| 0 - 500 | 778606 | 761026 | 713161 | 529299 |

Table 5: Number of events dependence on P_{t56} and $\Delta\phi$ for $200 \leq P_{t\gamma} \leq 240 \text{ GeV}/c$ and $P_{tCUT}^{clust} = 5 \text{ GeV}/c$ for $L_{int}=3fb^{-1}$

| P_{t56} (GeV/c) | $\Delta\phi_{max}$ | | | |
|----------------------|--------------------|------|------|------|
| | 180° | 15° | 10° | 5° |
| 0 - 5 | 369 | 369 | 369 | 369 |
| 5 - 10 | 563 | 563 | 563 | 562 |
| 10 - 15 | 217 | 217 | 217 | 217 |
| 15 - 20 | 56 | 56 | 56 | 56 |
| 20 - 25 | 20 | 20 | 20 | 18 |
| 25 - 30 | 9 | 9 | 9 | 7 |
| 30 - 40 | 7 | 7 | 7 | 6 |
| 40 - 50 | 6 | 6 | 6 | 5 |
| 50 - 100 | 10 | 10 | 10 | 10 |
| 100 - 300 | 8 | 8 | 8 | 8 |
| 300 - 500 | 0 | 0 | 0 | 0 |
| 0 - 500 | 1264 | 1264 | 1264 | 1257 |

Table 6: Number of events dependence on $\Delta\phi_{max}$ and on $P_{t\gamma}$ for $L_{int} = 3 \text{ fb}^{-1}$.
 $P_{tCUT}^{clust} = 5 \text{ GeV}/c$ (summary)

| $P_{t\gamma}$ (GeV/c) | $\Delta\phi_{max}$ | | | |
|--------------------------|--------------------|--------|--------|--------|
| | 180° | 15° | 10° | 5° |
| 40 - 50 | 778606 | 761026 | 713161 | 529299 |
| 100 - 120 | 22170 | 22143 | 22038 | 20786 |
| 200 - 240 | 1264 | 1264 | 1264 | 1257 |
| 300 - 360 | 212 | 212 | 212 | 212 |

Since the last lines in Tables 1, 2 and 4, 5 contain an important information on $\Delta\phi$ dependence of the total number of events, we supply these tables with the summarizing Tables 3 and 6. They include more intervals of P_t^γ and contain analogous numbers of events that can be collected in different $\Delta\phi$ intervals for two different P_t^{clust} cuts at $L_{int} = 3 fb^{-1}$ (one month of LHC continuous running at low luminosity).

2.2 P_t^γ and η^γ dependence of rates.

Since there are two main objects for experimental registration during the calibration procedure, namely a photon and a jet, we shall present here the number of events predicted by PYTHIA simulation with cuts defined by (1) for different intervals of P_t^γ and η^γ . The lines of Table 7 correspond to P_t^γ -intervals while the columns — to η^γ -intervals. The last column of this table contains the total number of events in the whole ECAL (at $L_{int} = 3 fb^{-1}$) η^γ -region $0 < |\eta^\gamma| < 2.61$ for a given P_t^γ -interval. We see from here that the events number decreases fastly with the P_t^γ growth (by more than 50% for each following interval) while for the fixed P_t^γ -interval there are no big changes with the variation of η^γ . Since $L_{int} = 3 fb^{-1}$ corresponds approximately to one month of LHC continuous running, we conclude that these rates demonstrate that, in principle, there would

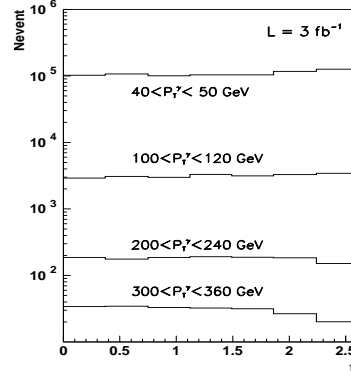


Fig. 1: η -dependence of rates for different P_t^γ -intervals

Table 7: Rates for $L_{int} = 3 fb^{-1}$ for different intervals of P_t^γ and η^γ ($P_t^{clust} = 5 GeV/c$ and $\Delta\phi \leq 15^\circ$).

| P_t^γ (GeV/c) | η^γ intervals | | | | | | | all η^γ 0.0-2.6 |
|-------------------------|-------------------------|---------|---------|---------|---------|---------|---------|------------------------------|
| | 0.0-0.4 | 0.4-0.7 | 0.7-1.1 | 1.1-1.5 | 1.5-1.9 | 1.9-2.2 | 2.2-2.6 | |
| 40 – 50 | 102656 | 107148 | 100668 | 103903 | 103499 | 116674 | 126546 | 761027 |
| 50 – 60 | 43905 | 41729 | 41074 | 45085 | 42974 | 47640 | 50310 | 312697 |
| 60 – 70 | 18153 | 18326 | 19190 | 20435 | 20816 | 19432 | 23650 | 140005 |
| 70 – 80 | 9848 | 10211 | 9963 | 10166 | 9951 | 11397 | 10447 | 71984 |
| 80 – 90 | 5287 | 5921 | 5104 | 5823 | 5385 | 6067 | 5923 | 39509 |
| 90 – 100 | 2899 | 3033 | 3033 | 3326 | 3119 | 3265 | 3558 | 22234 |
| 100 – 120 | 2908 | 3091 | 2995 | 3305 | 3133 | 3282 | 3429 | 22143 |
| 120 – 140 | 1336 | 1359 | 1189 | 1346 | 1326 | 1499 | 1471 | 9525 |
| 140 – 160 | 624 | 643 | 626 | 674 | 706 | 614 | 668 | 4555 |
| 160 – 200 | 561 | 469 | 557 | 555 | 519 | 555 | 557 | 3774 |
| 200 – 240 | 187 | 176 | 186 | 192 | 187 | 185 | 151 | 1264 |
| 240 – 300 | 103 | 98 | 98 | 98 | 100 | 92 | 74 | 665 |
| 300 – 360 | 34 | 34 | 33 | 32 | 31 | 27 | 20 | 212 |
| 40 – 360 | 188517 | 192274 | 184734 | 194957 | 191761 | 210742 | 226819 | 1389484 |

be quite enough number of events for the jet mass scale setting and successful calibration of HCAL. Fig. 1 gives a compact illustration of rates for four P_t^γ -intervals, considered here, completely contained in these regions, while column HE+HF gives the number of the events where the jet covers both the HE and HF regions. From these tables we can see what number

and it shows a very weak dependence on η^γ (or better to speak about their independence on η^γ).

2.3 Estimation of " $\gamma + Jet$ " events rates for HB, HE and HF regions.

Since the jet is a wide spread object, the η^{jet} dependence of rates for different P_t^γ -intervals will be presented in a different way than in Table 7. Namely, Tables 8–11 include the rates of events for different η^{jet} intervals, covered by the barrel, endcap and forward (HB, HE and HF) parts of HCAL and for different P_t^{Jet} intervals (for a case of $L_{int} = 3 fb^{-1}$). The selection cuts are taken as those of Section 3.2 of [1] specified by the following values of cuts parameters:

Table 8: Selection 1. $\Delta P_t^{jet}/P_t^{jet} = 0.00$

| P_t^γ | HB | HB+HE | HE | HE+HF | HF |
|--------------|--------|--------|--------|--------|-------|
| 40 – 50 | 260259 | 211356 | 141759 | 102299 | 45354 |
| 50 – 60 | 108827 | 89126 | 55975 | 41553 | 17216 |
| 60 – 70 | 49585 | 40076 | 25172 | 18153 | 7019 |
| 70 – 80 | 25506 | 20897 | 12881 | 9679 | 3021 |
| 80 – 90 | 14083 | 11720 | 7529 | 4873 | 1304 |
| 90 – 100 | 7261 | 7054 | 4142 | 2924 | 853 |
| 100 – 120 | 7703 | 6913 | 4013 | 2926 | 588 |
| 120 – 140 | 3372 | 2977 | 1805 | 1164 | 207 |
| 140 – 160 | 1650 | 1481 | 865 | 509 | 50 |
| 160 – 200 | 1493 | 1137 | 708 | 396 | 40 |
| 200 – 240 | 503 | 406 | 242 | 107 | 6 |
| 240 – 300 | 287 | 215 | 122 | 40 | 1 |
| 300 – 360 | 96 | 73 | 35 | 8 | 0 |
| 40 – 360 | 480538 | 393378 | 255266 | 184642 | 75660 |

Table 9: Selection 1. $\Delta P_t^{jet}/P_t^{jet} \leq 0.10$

| P_t^γ | HB | HB+HE | HE | HE+HF | HF |
|--------------|--------|-------|--------|-------|--------|
| 40 – 50 | 341043 | 55160 | 263629 | 26653 | 74534 |
| 50 – 60 | 144955 | 20396 | 108765 | 9300 | 29281 |
| 60 – 70 | 65525 | 8541 | 49412 | 3907 | 12621 |
| 70 – 80 | 34155 | 4093 | 25918 | 1957 | 5860 |
| 80 – 90 | 19224 | 1961 | 14741 | 804 | 2778 |
| 90 – 100 | 10258 | 1304 | 8394 | 536 | 1742 |
| 100 – 120 | 10859 | 1043 | 8357 | 545 | 1338 |
| 120 – 140 | 4618 | 509 | 3675 | 178 | 546 |
| 140 – 160 | 2325 | 222 | 1751 | 90 | 168 |
| 160 – 200 | 1971 | 147 | 1458 | 52 | 147 |
| 200 – 240 | 685 | 61 | 472 | 20 | 26 |
| 240 – 300 | 383 | 32 | 234 | 7 | 9 |
| 300 – 360 | 129 | 10 | 72 | 1 | 0 |
| 40 – 360 | 636418 | 93480 | 486788 | 44052 | 129050 |

$$P_{tCUT}^{isol} = 5 \text{ GeV}/c; \quad \epsilon_{CUT}^{\gamma} = 7\%; \quad \Delta\phi < 15^{\circ}; \quad P_{tCUT}^{clust} = 5 \text{ GeV}/c. \quad (2)$$

No any restrictions on other parameters are used. The first columns of these tables give the number of events with jets (found by LUCCELL jetfinding algorithm of PYTHIA), all particles of which are comprised completely (100%) in the barrel part (HB) and there is a 0% sharing of P_t^{jet} (ΔP_t^{jet}) between HB and neighbouring HE part of HCAL, i.e. $\Delta P_t^{jet} = 0$. Second columns of these tables contain a number of the events in which P_t of the jet is shared between HB and HE regions. The same sequence of restriction conditions takes place in the following columns. Thus, HE and HF columns include a number of events with the jets

Table 10: Selection 2. $\Delta P_t^{jet}/P_t^{jet} = 0.00$

| P_t^{γ} | HB | HB+HE | HE | HE+HF | HF |
|----------------|--------|-------|-------|-------|-------|
| 40 – 50 | 46972 | 32954 | 26114 | 16208 | 10041 |
| 50 – 60 | 23717 | 18911 | 13448 | 8367 | 5047 |
| 60 – 70 | 14384 | 9751 | 7469 | 4703 | 2386 |
| 70 – 80 | 8546 | 6733 | 4627 | 2960 | 1206 |
| 80 – 90 | 5653 | 4386 | 3107 | 1925 | 573 |
| 90 – 100 | 3326 | 3119 | 1900 | 1377 | 390 |
| 100 – 120 | 4157 | 3435 | 2271 | 1467 | 324 |
| 120 – 140 | 2183 | 1786 | 1185 | 710 | 134 |
| 140 – 160 | 1175 | 1005 | 635 | 362 | 31 |
| 160 – 200 | 1179 | 905 | 565 | 314 | 25 |
| 200 – 240 | 442 | 353 | 212 | 97 | 5 |
| 240 – 300 | 273 | 200 | 116 | 37 | 1 |
| 300 – 360 | 94 | 71 | 35 | 7 | 0 |
| 40 – 360 | 112111 | 83617 | 61686 | 38535 | 20163 |

Table 11: Selection 2. $\Delta P_t^{jet}/P_t^{jet} \leq 0.10$

| P_t^{γ} | HB | HB+HE | HE | HE+HF | HF |
|----------------|--------|-------|--------|-------|-------|
| 40 – 50 | 60113 | 7986 | 45388 | 3909 | 14894 |
| 50 – 60 | 31495 | 3631 | 25134 | 1971 | 7259 |
| 60 – 70 | 18326 | 2248 | 13139 | 968 | 4011 |
| 70 – 80 | 11385 | 1243 | 8741 | 573 | 2132 |
| 80 – 90 | 7614 | 633 | 5957 | 292 | 1145 |
| 90 – 100 | 4544 | 536 | 3886 | 280 | 865 |
| 100 – 120 | 5771 | 481 | 4434 | 278 | 689 |
| 120 – 140 | 2909 | 272 | 2370 | 94 | 352 |
| 140 – 160 | 1648 | 138 | 1246 | 65 | 111 |
| 160 – 200 | 1560 | 113 | 1162 | 38 | 115 |
| 200 – 240 | 600 | 53 | 416 | 17 | 23 |
| 240 – 300 | 362 | 30 | 220 | 6 | 8 |
| 300 – 360 | 126 | 10 | 71 | 1 | 0 |
| 40 – 360 | 146468 | 17374 | 112177 | 8492 | 31603 |

of the events can, in principle, be suitable for the most precise calibration procedure, carried out separately for HB, HE and HF parts of HCAL in different intervals of P_t^{jet} .

Less restrictive conditions, when up to 10% of the jet P_t are allowed to be shared between HB, HE and HF parts of HCAL, are given in Tables 9 and 11. Tables 8 and 9 correspond to the case of Selection 1 (see [1]). Tables 10 and 11 contain a number of events collected with addition of Selection 2 restriction, i.e. they include only the events with “isolated jets” (whose definition is given by (26) in the same Section 3.2 of [1]).

From Table 8, that corresponds to the most restrictive selection and gives the number of events most suitable for HCAL calibration, we see from the last summarizing lines that for the interval $40 < Pt^\gamma < 360 \text{ GeV}/c$ PYTHIA predicts around a half of million of events for HB and a quarter of million of events for HE per one month of continuous data taking at low LHC luminosity, while for HF it is expected to be less than 80 000 events per month.

One should keep in mind that the last columns in Tables 8–11 can not be taken as the final result here as we have not defined the meaning of sharing P_t^{jet} between the HF regions and the region with $|\eta| > 5$, i.e. close to a “beam-pipe” region. A more accurate estimation can be done here by finding events with jets in a wider region than the HF volume restricted by $3 < |\eta^{HF}| < 5$ and by calculation of a number of those events whose jets are contained in HF completely with all particles belonging to them.

3. STUDY OF FEATURES OF “ $\gamma + Jet$ ” EVENTS IN THE HCAL BARREL REGION.

In this section we shall study a specific sample of events that may be most suitable for HB calibration. It is a sample of events in which jets are completely (100%) contained in HB region, i.e. having 0% sharing of P_t^{jet} (at PYTHIA level of simulation) with HE. Below we shall call them “HB-events”. A particular set of these events for $P_t^{clust} = 5 \text{ GeV}/c$ is presented in the first column (HB) of Table 8. Here we shall use two different jetfinders, namely, LUCCELL from PYTHIA and UA1 (the last one is taken ⁴ from CMSJET [6]) for an equal foot determination of clusters and jets. The distributions of P_t^{clust} for generated events found by these two different jetfinders in two P_t^γ intervals, $40 < P_t^\gamma < 50 \text{ GeV}/c$ and $300 < P_t^\gamma < 360 \text{ GeV}/c$, are shown in Fig. 2 for $P_{tCUT}^{clust} = 30 \text{ GeV}/c$.

3.1 Influence of the P_{tCUT}^{clust} parameter on the photon and jet P_t balance and initial state radiation suppression.

Here we shall study correlation of P_t^{clust} with P_t^{ISR} proportional to $P_t/56$ for the fixed $\langle k_T \rangle$ (The influence of the $\langle k_T \rangle$ variation on the P_t^γ and P_t^{Jet} balance is discussed in [4]).

The banks of 1-jet “ $\gamma + Jet$ ” events gained from the already mentioned (in Section 2.1) results of PYTHIA generation of 10^7 signal “ $\gamma + Jet$ ” events in each of four P_t^γ intervals ($40 - 50$, $100 - 120$, $200 - 240$, $300 - 360 \text{ GeV}/c$) will be used here. The observables defined in Sections 3.1 and 3.2 of paper [1] will be restricted here by Selection 1 cuts (17) – (24) of Section 3.2 of [1] and the cut parameters defined by (1). The luminosity was chosen to be $L = 10^{33} \text{ cm}^2 \text{ sec}^{-1}$.

⁴In order to select events with P_t^{clust} value starting from $5 \text{ GeV}/c$ we have changed the P_t precluster threshold in the UA1 algorithm from $10 \text{ GeV}/c$, taken as default value, to $1.5 \text{ GeV}/c$. We also increase the cone radius in the UA1 algorithm from 0.5 to 0.7.

We have chosen two of these intervals with the extreme values of P_t^γ to illustrate the influence of the P_{tCUT}^{clust} parameter on the distributions of physical variables. The results of

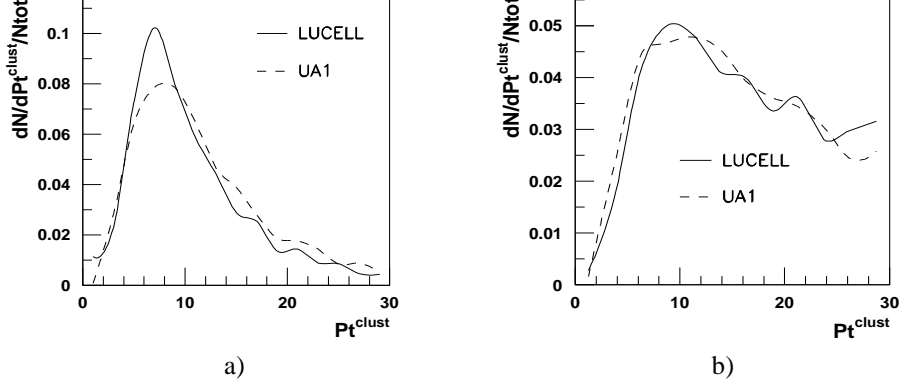


Fig. 2: P_t^{clust} -distribution in " $\gamma + Jet$ " events from two P_t^γ intervals: a) $40 < P_t^\gamma < 50 \text{ GeV}/c$ and b) $300 < P_t^\gamma < 360 \text{ GeV}/c$ with the same cut $P_{tCUT}^{clust} = 30 \text{ GeV}/c$.

P_{tCUT}^{clust} variation are shown in Fig. 3 for $40 < P_t^\gamma < 50 \text{ GeV}/c$ and in Fig. 4 for $300 < P_t^\gamma < 360 \text{ GeV}/c$. In these figures, in addition to three variables P_{t56} , $P_t^{\eta>5}$, P_t^{out} , already explained in Sections 2.2, 3.1 and 3.2 of [1], we present the distributions for other two variables, $P_t(O+\eta > 5)$ and $(1 - \cos\Delta\phi)$, which define the right-hand side of equation (29) of [1]. The distribution for the back-to-back $\Delta\phi$ angle (see (23) of [1]) which defines the second variable, is also presented in Figs. 3, 4.

The disbalance variable P_{t56} (defined by formula (3) of [1]) and both components of another disbalance measure $(P_t^\gamma - P_t^{jet})/P_t^\gamma$ (defined by formula (29) of [1]) as a sum of $(1 - \cos\Delta\phi)$ and $P_t(O+\eta > 5)$, as well as two others, P_t^{out} and $\Delta\phi$, show a tendency, as it is seen from Figs. 3 and 4, to become smaller with the restriction of the upper limit on the P_t^{clust} value. It means that the calibration precision may increase with decreasing P_{tCUT}^{clust} , which justifies the intuitive choice of this new variable in Section 3 of [1]. The origin of this improvement becomes clear from the P_{t56} density plot, which demonstrates suppression of P_{t56} (or P_t^{ISR}) with implying a more restrictive cut on P_t^{clust} .

The comparison of Fig. 3 (for $40 < P_t^\gamma < 50 \text{ GeV}/c$) and Fig. 4 (for $300 < P_t^\gamma < 360 \text{ GeV}/c$) shows that a degree of back-to-backness of the photon and jet P_t vectors in the ϕ -plane increases with increasing P_t^γ . At the same time P_t^{out} and P_t^{ISR} distributions become wider, while the $P_t^{\eta>5}$ distribution practically does not depend on P_t^γ and P_t^{clust} .

It should be mentioned that the results presented in Figs. 3 and 4 were obtained with the LUCCELL jetfinder of PYTHIA ⁵.

⁵The results obtained with both jetfinders and P_t^γ and P_t^{Jet} balance will be discussed in [2, 3] in more detail

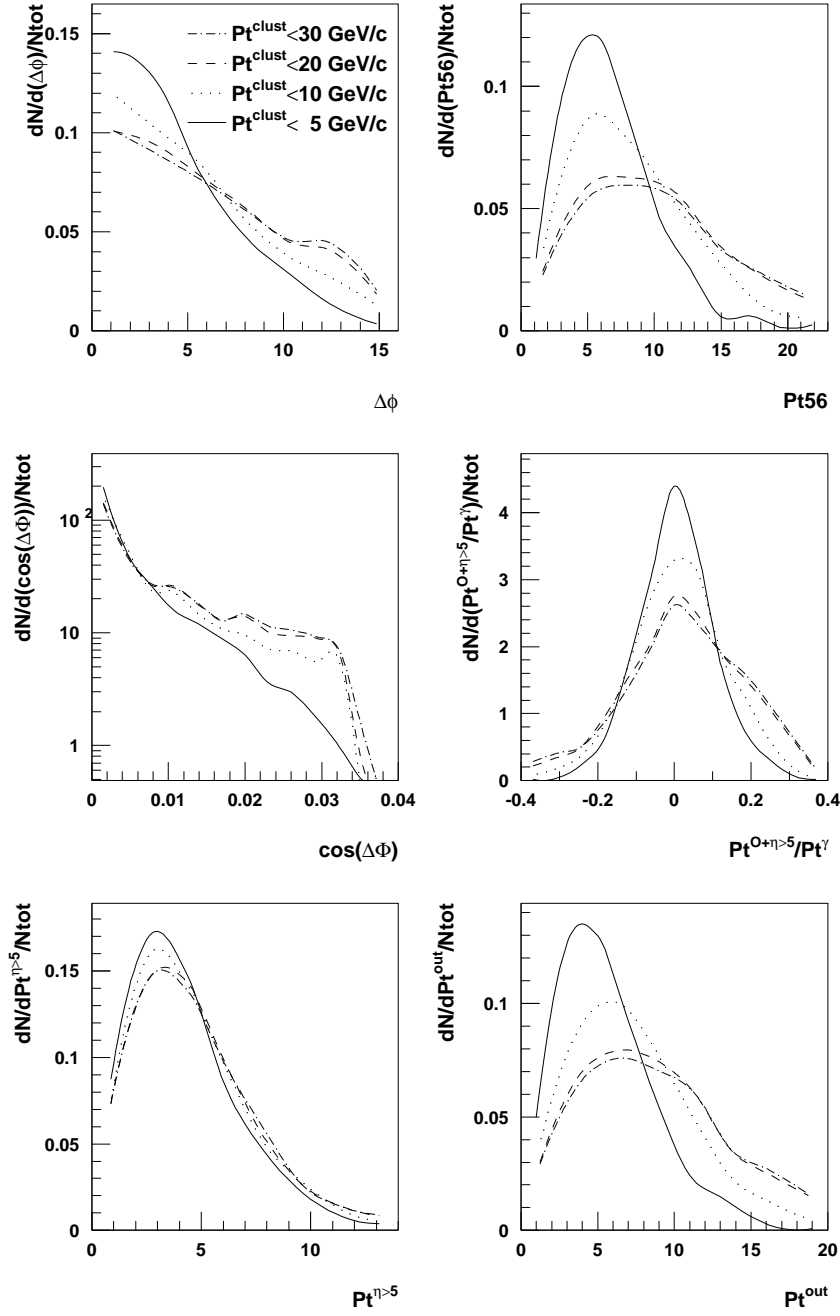


Fig. 3: LUCCELL algorithm, $\Delta\phi < 15^\circ$, $40 < P_t^\gamma < 50 \text{ GeV}/c$. Selection 1.

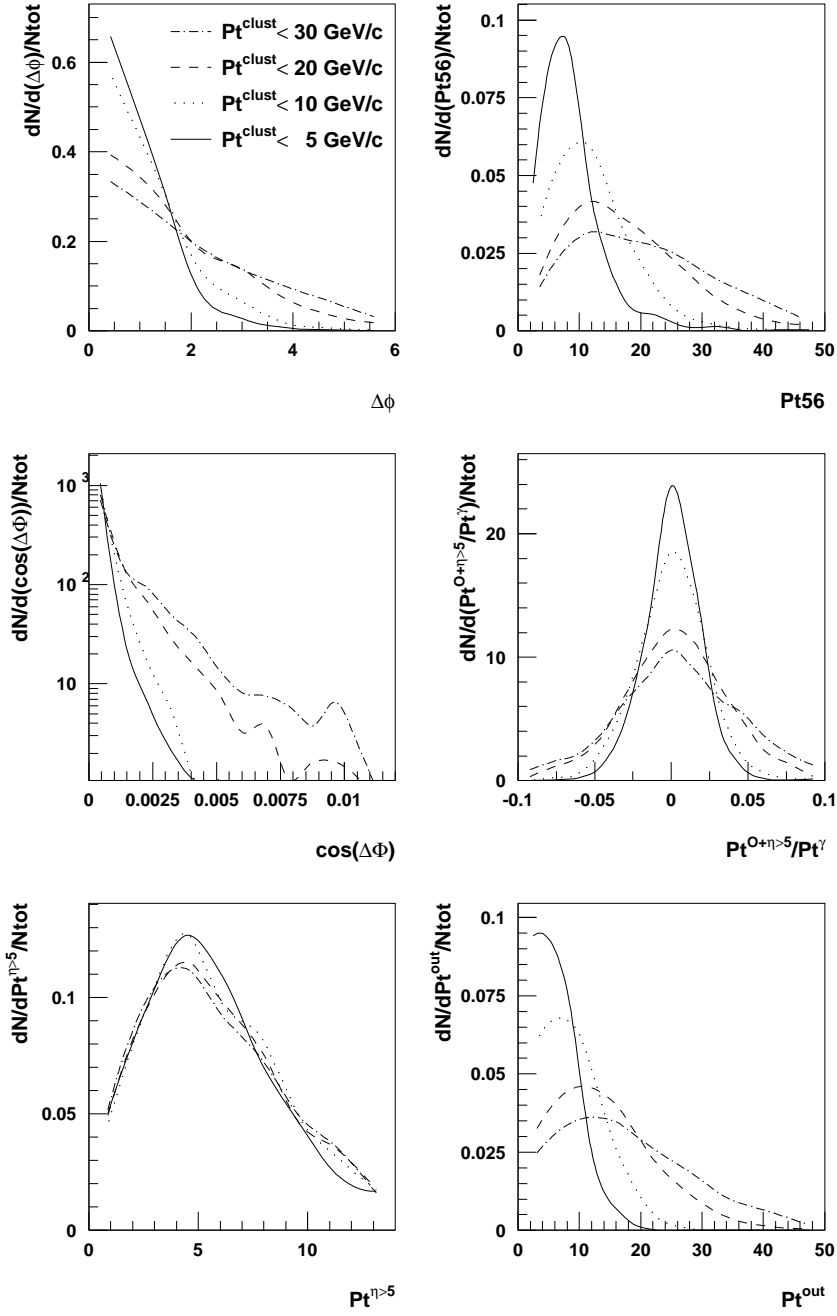


Fig. 4: LUCCELL algorithm, $\Delta\phi < 15^\circ$, $300 < P_t^\gamma < 360 \text{ GeV}/c$. Selection 1.

3.2 Jetfinders and P_t structure of jets in $\eta - \phi$ space.

In order to understand well the calibration procedure of " $\gamma + Jet$ " events, it is useful to keep control over some principal characteristics of jets and of the P_t activity in the space around them. The left-hand columns of Figs. 5 and 6 represent jet radius $R^{jet}(\eta, \phi)$ distributions in these HB-events for the intervals: $40 < P_t^\gamma < 50 \text{ GeV}/c$ and $300 < P_t^\gamma < 360 \text{ GeV}/c$, respectively. We have chosen the jet radius counted from the initiator cell (ic) to be restricted by $R_{ic}^{jet} = 0.7$ for the LUCCELL and UA1 jetfinders.

From the left-hand side plots in Figs. 5 and 6 we see that both jetfinders give close enough results for R_{gc}^{jet} distribution. In these plots the radius in $\eta - \phi$ space is counted from the gravity center (gc). The detailed information about averaged values of the jet radius for four P_t^γ -intervals will be presented in the tables of Appendices 1–4 of [3] ⁶.

Let us now consider the question, how the transverse momentum is distributed inside a jet. Let us divide the jet radius $R^{jet}(\eta, \phi) \equiv R$ into a set of ΔR bins and calculate the vector sums of cells P_t in each ΔR_{bin} ring. Normalized to P_t^{Jet} , the modulus of this vector sum, denoted by P_t^{bin} , would give the value that tells us what portion of P_t^{Jet} is contained in the ring of size ΔR_{bin} . Its variation with the distance R counted from the center of gravity of the jet is shown in the right-hand columns of Figs. 5 and 6.

From these figures we can conclude that the LUCCELL and UA1 jetfinders lead to equally P_t -densed central part inside the jet.

3.3 P_t distribution inside and outside a jet.

Now let us see how the volume outside the jet, (i.e. calorimeter cells outside the jet cone), may be populated by P_t in these HB " $\gamma + Jet$ " events. For this purpose we calculate a vector sum \vec{P}_t^{sum} of individual transverse momenta of $\Delta\eta \times \Delta\phi$ cells, included by a jetfinder into a jet as well as of cells in a larger volume that surrounds a jet. In the last case this procedure in some sense can be viewed as some straightforward enlarging of the jet radius in the $\eta - \phi$ space.

The figures that represent the ratio P_t^{sum}/P_t^γ , as a function of the distance $R(\eta, \phi)$ counted from the jet gravity center towards its boundary and further into space outside the jet are shown in the left-hand columns of Figs. 7 and 8 for a case when all jet particles are kept in the jet, while the case of the magnetic field effect account (i.e. when the contribution from charged particles with $P_t \leq 0.8 \text{ GeV}/c$ is removed ⁷ from the total jet P_t in a case of HB events) is shown in the left-hand columns of Figs. 9 and 10.

From these figures we see that the jet surrounding space is found to be far from being an empty one in the case of " $\gamma + Jet$ " events considered here. We also see that an average value of the total P_t^{sum} increases with increasing the volume around the jet and it exceeds P_t^γ at $R = 0.7 - 0.8$ when all particles are included into the jet (see Figs. 7 and 8), while in the case of rejected charged particles with $P_t^{ch} < 0.8 \text{ GeV}/c$ only about 95 – 97% of P_t^{Jet} are collected at $R = 0.7 - 0.8$.

From the right-hand column of Fig. 7 we see that when all particles are included into the jet, the following disbalance measure:

⁶From there one can see a weak dependence of the jet radius on $P_t^{Jet}(\approx P_t^\gamma)$ for both UA1 and LUCCELL algorithms

⁷See [5]

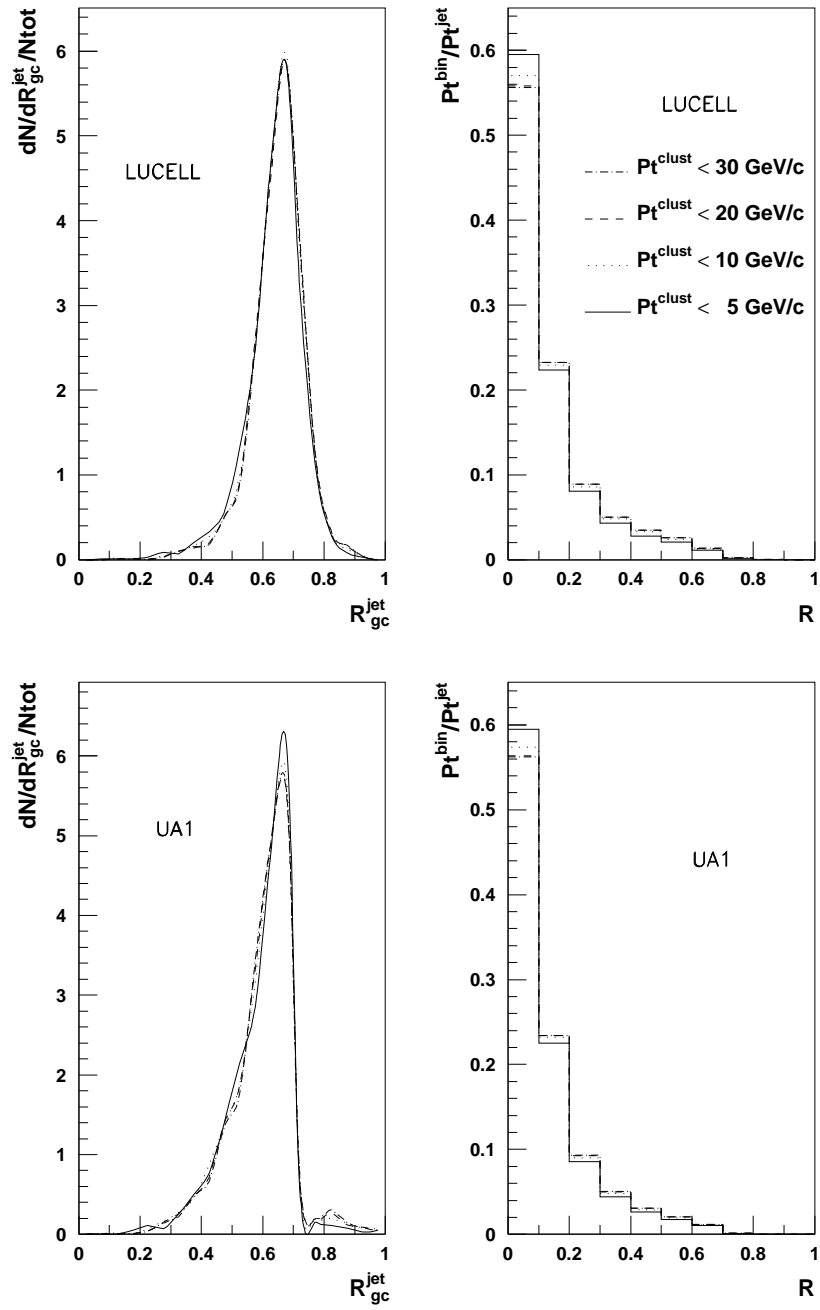


Fig. 5: LUCCELL and UA1 algorithms, $\Delta\phi < 15^\circ$, $40 < P_t^\gamma < 50 \text{ GeV}/c$. Selection 1.

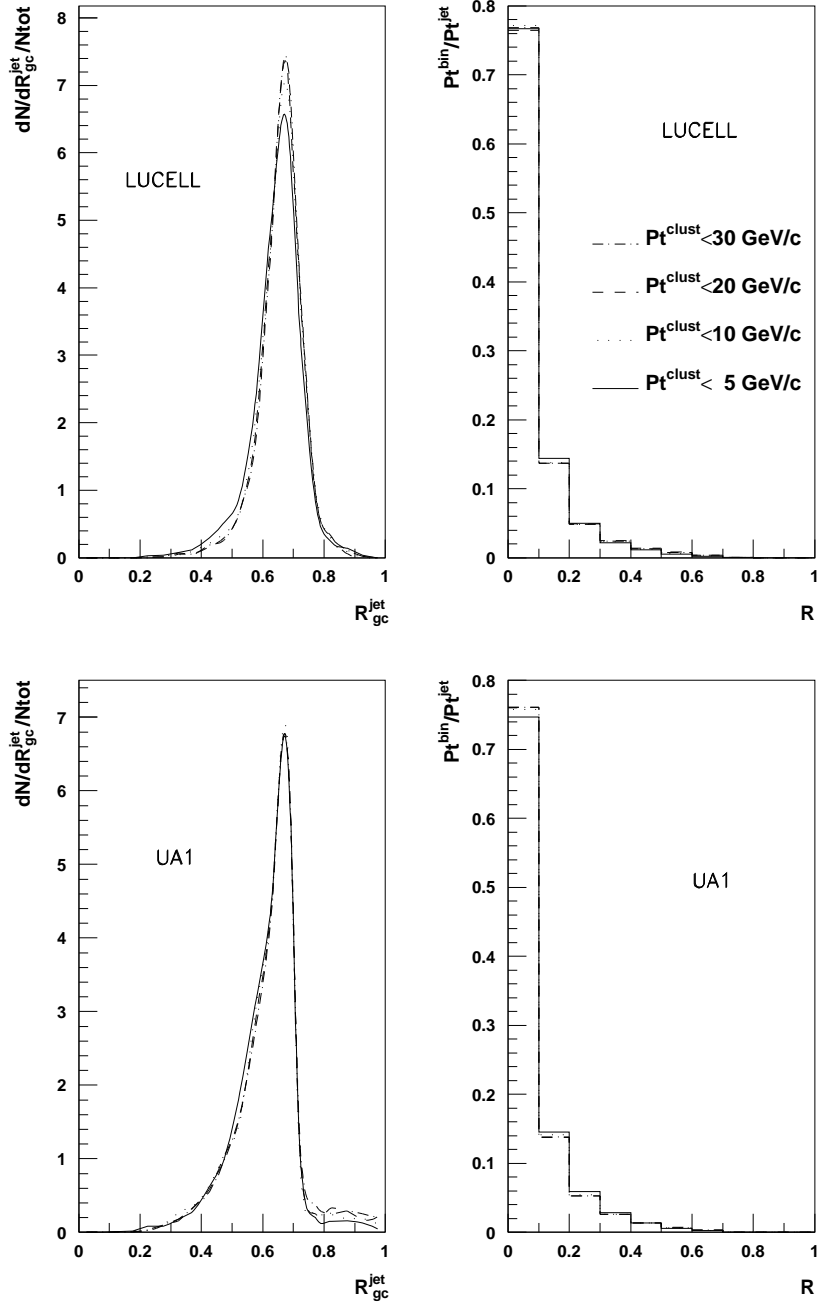


Fig. 6: LUCCELL and UA1 algorithms, $\Delta\phi < 15^\circ$, $300 < P_t^\gamma < 360 \text{ GeV}/c$. Selection 1.

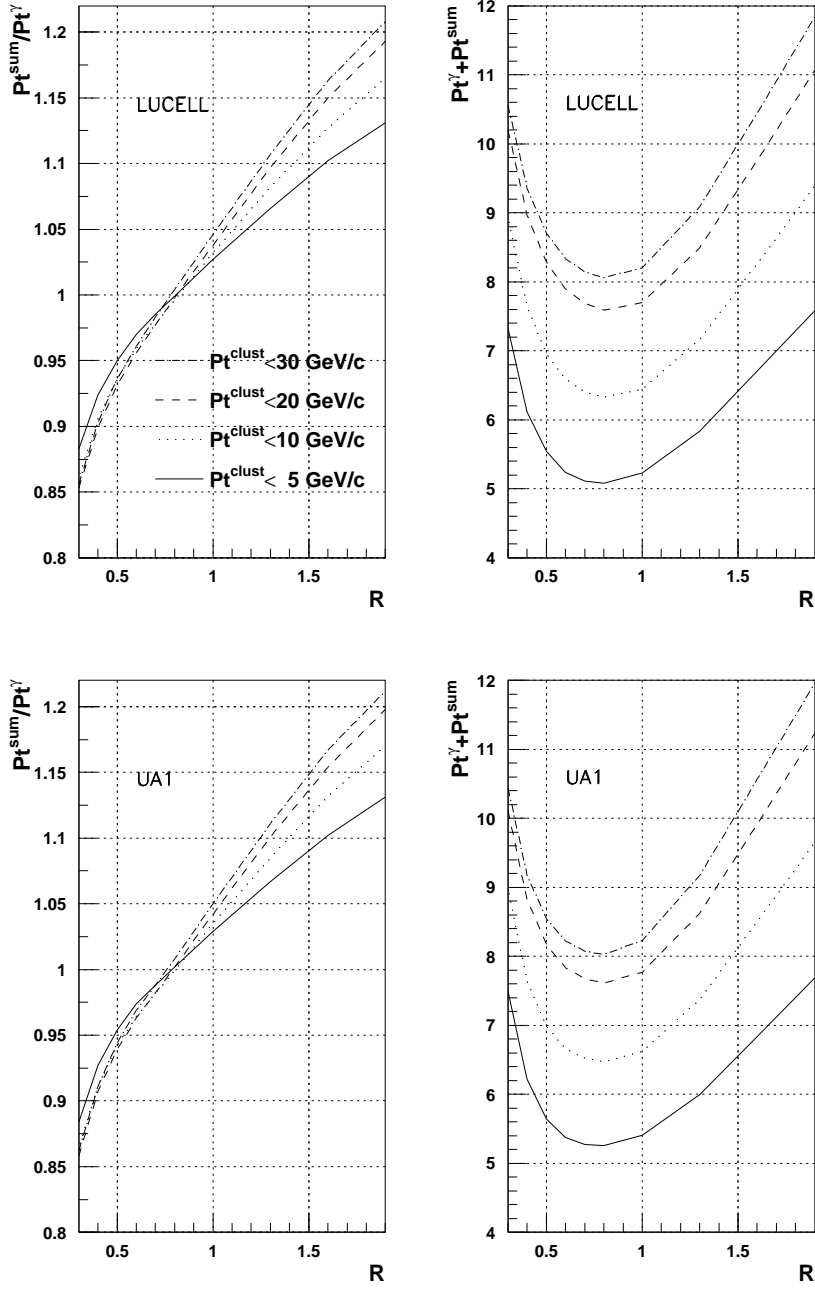


Fig. 7: LUCCELL and UA1 algorithms, $\Delta\phi < 15^\circ$, $40 < P_t^\gamma < 50 \text{ GeV}/c$

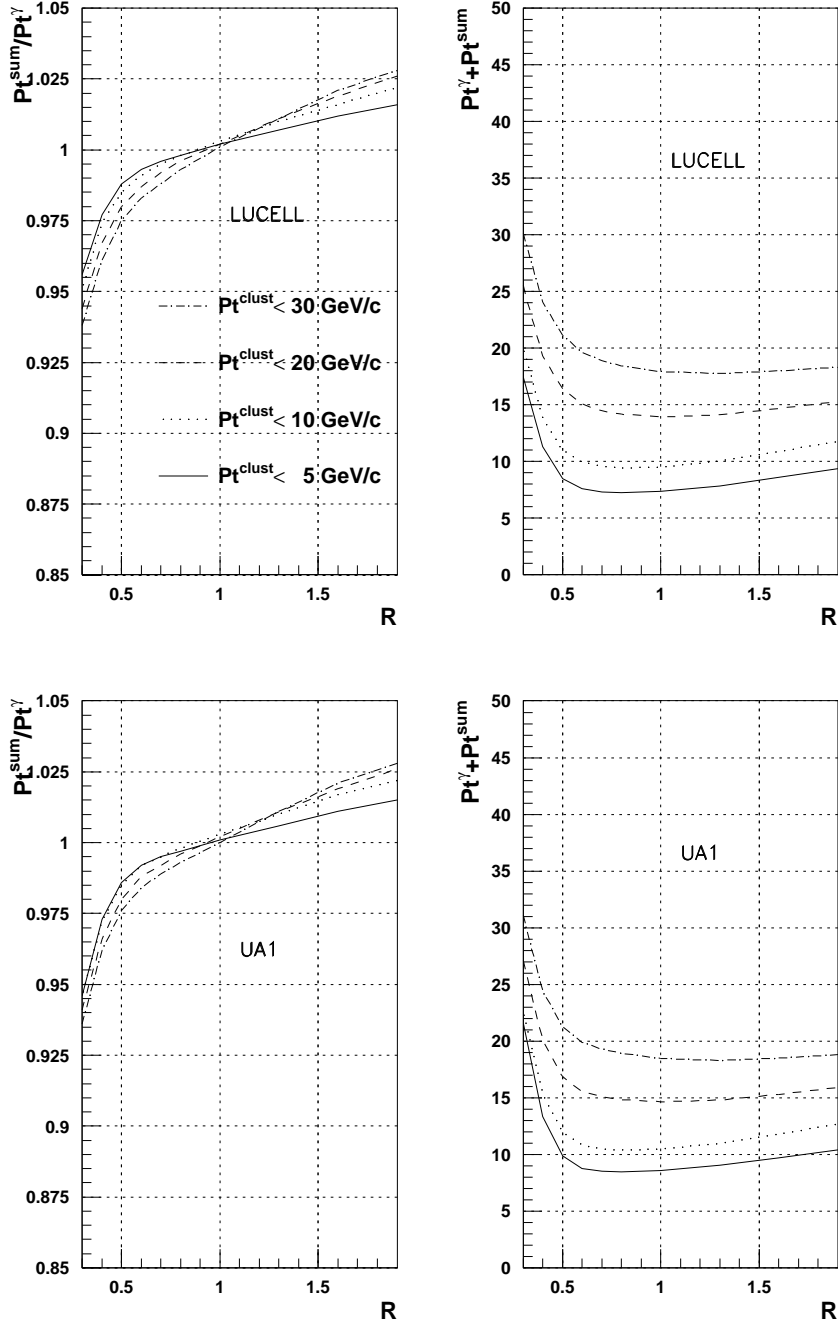


Fig. 8: LUCCELL and UA1 algorithms, $\Delta\phi < 15^\circ$, $300 < P_t^\gamma < 360 \text{ GeV}/c$

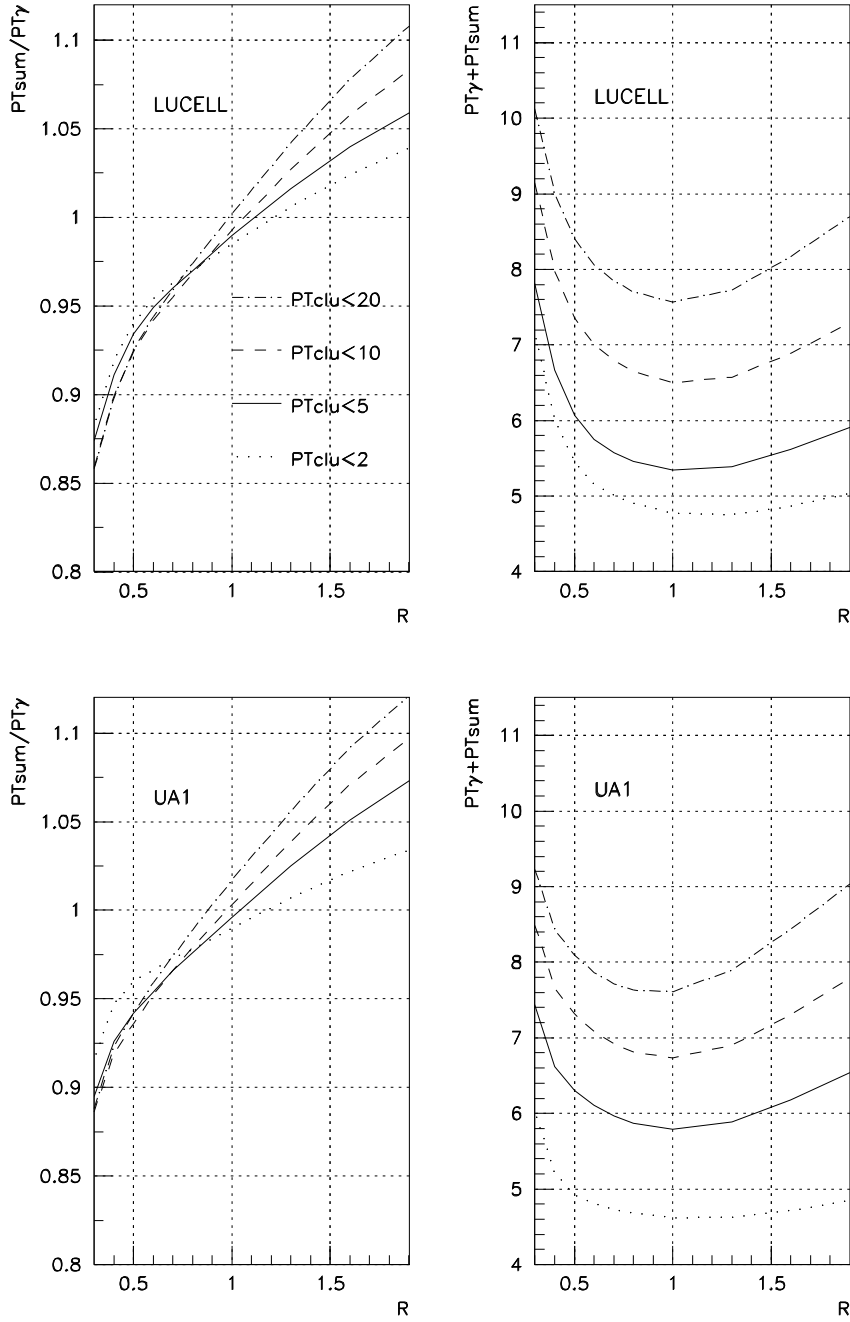


Fig. 9: LUCCELL and UA1 algorithms, $\Delta\phi < 15^\circ$, $40 < P_t^\gamma < 50 \text{ GeV}/c$, $P_{tch}^{jet} > 0.8 \text{ GeV}/c$.

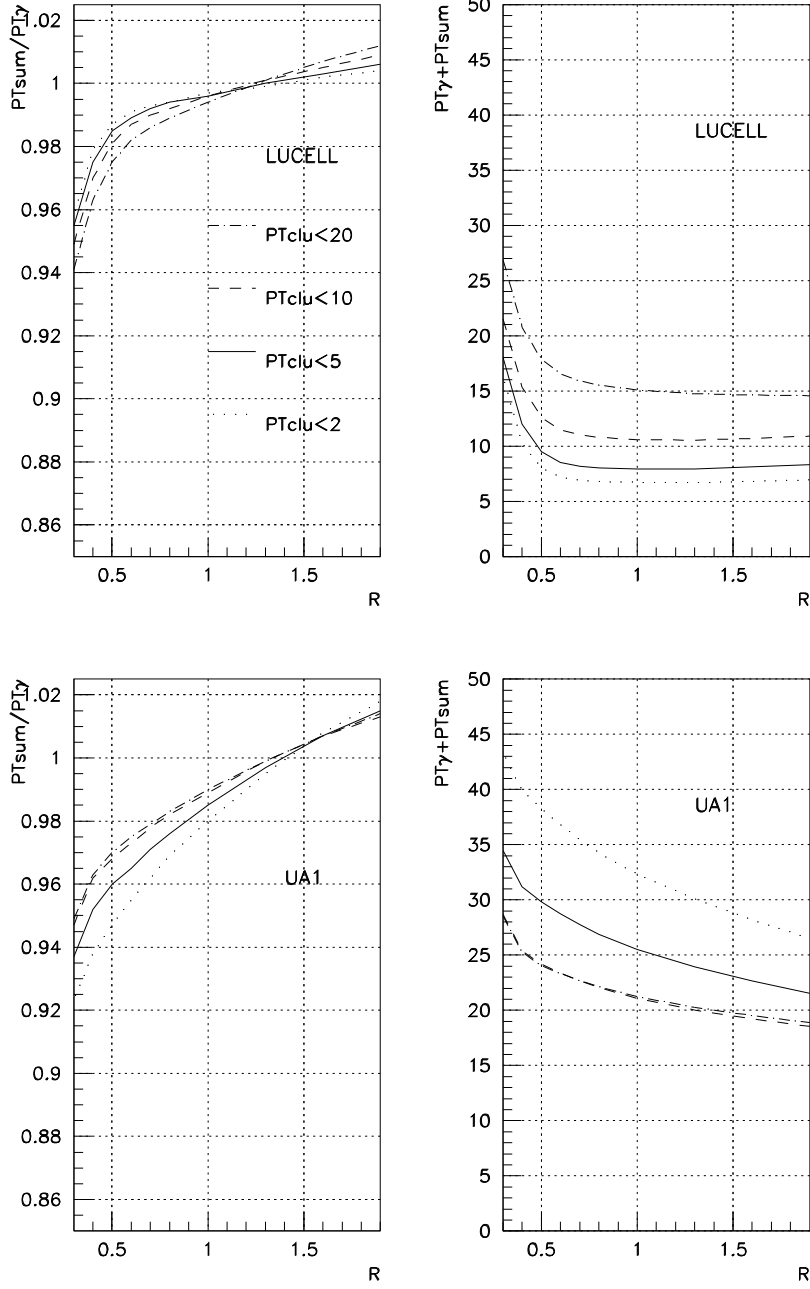


Fig. 10: LUCCELL and UA1 algorithms, $\Delta\phi < 15^\circ$, $300 < P_{t\gamma} < 360 \text{ GeV}/c$, $P_{t_{ch}}^{jet} > 0.8 \text{ GeV}/c$.

$$P_t^{\gamma+sum} = \left| \vec{P}_t^\gamma + \vec{P}_t^{sum} \right| \quad (3)$$

achieves its minimum at $R \approx 0.7 - 0.8$ for both LUCCELL and UA1 algorithms. From Figs. 9 and 10 we see that with account of the magnetic field effect on charged particles with $P_t^{ch} < 0.8 \text{ GeV}/c$ the minimum of $P_t^{\gamma+sum}$ is achieved at larger values of $R \approx 1.0$ again for both LUCCELL and UA1 jetfinders.

The value of $P_t^{\gamma+sum}$ continues to grow rapidly with increasing R after the point $R=1$ for $40 < P_t^\gamma < 50 \text{ GeV}/c$ (see Figs. 7, 9), while for higher P_t^γ (see Figs. 8, 10 for the $300 < P_t^\gamma < 360 \text{ GeV}/c$ interval) the ratio P_t^{sum}/P_t^γ and the disbalance measure $P_t^{\gamma+sum}$ increase more slowly with increasing R after the point $R=0.7$. This means that at higher P_t^γ (or P_t^{Jet}) the topology of " $\gamma + Jet$ " events becomes more pronounced and we get a cleaner picture of an "isolated" jet. This feature clarifies the motivation of introduction of two criteria "Selection 2", (see "Point 8") and of "Selection 3" (see "Point 9") in Section 3.2 of [1] for selection of events with "isolated jets".

4. SUMMARY

From the study in Section 2.1 we see that the PYTHIA simulation predicts that most " $\gamma + Jet$ " events at LHC energies may have the vectors \vec{P}_t^γ and \vec{P}_t^{Jet} being back-to-back within $\Delta\phi < 15^\circ$ (about 66% for $40 \leq P_t^\gamma \leq 50 \text{ GeV}/c$ and greater than 99% for $P_t^\gamma \geq 200 \text{ GeV}/c$). At the same time, as it is seen from Table 1, a substantial part of the P_t^{ISR} ($\approx P_t^{56}$) spectrum spreads out in the interval $0 < P_t^{56} < 20 \text{ GeV}/c$, having the peak inside the $5 < P_t^{56} < 10 \text{ GeV}/c$ interval and noticeable tails (about of 5 – 10% of number of events) extending to $P_t^{56} = 40 \text{ GeV}/c$ not only for $\Delta\phi < 15^\circ$ but also for the smaller $\Delta\phi < 10^\circ$ and $\Delta\phi < 5^\circ$ intervals. From here we can conclude that the use of only one traditional $\Delta\phi$ cut does not help much to reduce the P_t^{ISR} contribution at LHC energies. It is most obvious from Table 2, where we find that at high P_t^γ ($200 < P_t^\gamma < 240 \text{ GeV}/c$) more that 99% of events belong to the $\Delta\phi < 15^\circ$ interval. Most of these events lay within the $0 < P_t^{56} < 50 \text{ GeV}/c$ interval. Even for $\Delta\phi < 5^\circ$, a considerable part of the spectrum belongs to the interval $0 < P_t^{56} < 40 \text{ GeV}/c$. Thus, a decrease in $\Delta\phi$ has, in fact, no big influence on the P_t^{ISR} spectrum and it cannot be useful to reduce the number of events with essential amount of initial state radiation at LHC energies.

In Section 3 the efficiency of P_t^{clust} for ISR suppression was demonstrated. From Figs. 3 and 4 we see that the distribution for P_t^{56} becomes narrower with decreasing P_t^{clust} . Analogous behavior is shown by the P_t^{out} (as P_t^{clust} is a part of P_t^{out}) spectra. These figures serve as an illustration for a more detailed study of P_t^{clust} influence on P_t^γ and P_t^{Jet} balance, which will be presented in our next papers [2–4].

A strict limitation of the P_t^{clust} parameter, introduced in Section 3.2 of [1], (by $\approx 5 - 10 \text{ GeV}/c$) improves this tendency. Simultaneously, due to this limitation, one can noticeably reduce radiation in the initial state (compare Tables 1, 4 and 2, 5), which leads to decreasing P_t^γ and P_t^{Jet} disbalance.

From Section 2.3 (Table 8) we see that even with the restrictive cuts mentioned there one can expect around a half million of events for HB, a quarter million of events for HE, and less than 80 000 events for the HF part and $L_{int} = 3 \text{ fb}^{-1}$ (i.e. per month of continuous data taking at low LHC luminosity) for interval $40 < P_t^\gamma < 360 \text{ GeV}/c$ for the sample of events that corresponds to 0% P_t sharing between HCAL parts. Despite those cuts the number of

events for the HCAL part above, in principle, can be quite sufficient for successful jet energy scale setting and HCAL calibration.

5. ACKNOWLEDGEMENTS

We are greatly thankful to D. Denegri for having offered this theme to study, fruitful discussions and permanent support and encouragement. It is a pleasure for us to express our recognition for helpful discussions to P. Aurenche, M. Dittmar, M. Fontannaz, J.Ph. Guillet, M.L. Mangano, E. Pilon, H. Rohringer, S. Tapprogge and J. Womersley.

References

- [1] D.V. Bandourin, V.F. Konoplyanikov, N.B. Skachkov. “Jet energy scale setting with $\gamma + Jet$ ” events at LHC energies. Generalities, selection rules”. JINR Communication, JINR, Dubna, 2000-
- [2] D.V. Bandourin, V.F. Konoplyanikov, N.B. Skachkov. “Jet energy scale setting with $\gamma + Jet$ ” events at LHC energies. Minijets and cluster suppression and $P_t^\gamma - P_t^{Jet}$ disbalance”. JINR Communication, JINR, Dubna, 2000-
- [3] D.V. Bandourin, V.F. Konoplyanikov, N.B. Skachkov. “Jet energy scale setting with $\gamma + Jet$ ” events at LHC energies. Selection of events with a clean $\gamma + Jet$ topology and $P_t^\gamma - P_t^{Jet}$ disbalance”. JINR Communication, JINR, Dubna, 2000-
- [4] D.V. Bandourin, V.F. Konoplyanikov, N.B. Skachkov. “Jet energy scale setting with $\gamma + Jet$ ” events at LHC energies. Detailed study of the background suppression”. JINR Communication, JINR, Dubna, 2000-
- [5] CMS Tracker project, Technical Design Report, CERN/LHCC 98–6, CMS TDR 5, p. 467.
- [6] S. Abdullin, A. Khanov, N. Stepanov, CMS Note CMS TN/94–180 “CMSJET”.